Pure Appl. Chem., Vol. 80, No. 6, pp. 1195–1210, 2008.
doi:10.1351/pac200880061195

Capabilities of chemical simulation methods in the elucidation of structure and dynamics of solutions*

Thomas S. Hofer‡, Andreas B. Pribil, and Bernhard R. Randolf

Theoretical Chemistry Division, Institute of General, Inorganic and Theoretical Chemistry, University of Innsbruck, Innrain 52a, A-6020 Innsbruck, Austria

Abstract: As a result of recent methodological developments in connection with enhanced computational capacity, theoretical methods have become increasingly valuable and reliable tools for the investigation of solutions. Simulation techniques utilizing a quantum mechanical (QM) approach for the treatment of the chemically most relevant region so-called hybrid quantum mechanical/molecular mechanical (QM/MM) simulations have reached a level of accuracy that often equals or may even surpass experimental methods. The latter is true in particular whenever ultrafast (i.e., picosecond) dynamics prevail, such as in labile hydrates or structure-breaking systems.

The recent development of an improved QM/MM framework, the quantum mechanical charge field (QMCF) ansatz, enables a broad spectrum of solute systems to be elucidated. As this novel methodology does not require any solute solvent potential functions, the applicability of the QMCF method is straightforward and universal. This advantage is bought, however, at the price of a substantial increase of the QM subregion, and an attendant increase in computational periods to levels of months, and even a year, despite parallelizing high-performance computing (HPC) clusters.

Molecular dynamics (MD) simulations of chemical systems showing increasing complexity have been performed, and demonstrate the superiority of the QMCF ansatz over conventional QM/MM schemes. The systems studied include Pd^{2+}, Pt^{2+}, and Hg_2^{2+}, as well as composite anions such as PO_4^{3-} and ClO_4^-.

Keywords: QM/MM MD simulation; QMCF MD simulation; ion solvation; hydration structure; hydration dynamics.

INTRODUCTION

The field of solution chemistry has gained an increasingly important position in chemical research [1–4], as the liquid state is by far the most relevant one in chemistry and also of great importance in related disciplines such as physics, biology, and geology. For this reason, solution chemistry is not restricted to an exclusive part of chemistry—the majority of chemical reactions and basically all biological processes take place in liquid phase and are strongly dependent on the properties of the solvent and its interaction with all present species. Typical solvate systems range from ionic hydrates, inorganic and metal–organic complexes, and (bio)organic molecules to macromolecules such as nucleic acids, pro-

*Paper based on a presentation at the 30th International Conference on Solution Chemistry (ICSC 30), 16–20 July 2007, Perth, Australia. Other presentations are published in this issue, pp. 1195–1347.

‡Corresponding author: Tel.: +43-512-507-5161; Fax: +43-512-507-2714; E-mail: t.hofer@uibk.ac.at

teins, and composite membrane layers, thus covering inorganic and organic chemistry as well as biochemistry (which is strongly linked to pharmaceutical science) and geochemistry, including the case where nonambient conditions such as high temperatures or pressures act on the liquid.

The theoretical models utilized in the underlying interpretation of the experimental results depend on concepts of physical chemistry like statistical thermodynamics [5,6] and the theory of intermolecular forces [7]. This relation became more evident after the technological resources allowed a computational treatment of condensed chemical systems, even at the level of quantum mechanics (QM), thereby expanding applied theoretical chemistry to the liquid state [8–10].

As solution chemistry is a multidisciplinary field of research, a variety of experimental as well as theoretical methods are being employed to investigate solvation processes. Methods relying on X-ray radiation and neutron beams have been applied to determine structural properties [1,2,11–13] while other methods like NMR [3,14] and a variety of other spectroscopic methods enable the investigation of dynamical aspects [15–17]. One of the most active fields is the investigation of the solvation structure of ions in solutions [1,3,11,14] as ionic solvates show a broad spectrum of properties and thus chemical behavior.

One of the most illustrative properties to demonstrate the diversity of ion solvation is the mean ligand residence time (MRT) of first-shell ligands in aqueous solution being in the order of 300 years for Ir(III) and lower than 200 ps in the case of Cs(I) [3,14], thus covering a range of 20 orders of magnitude. The latter value is an upper limit deduced from IQENS (incoherent quasielastic neutron scattering) experiments, as the actual exchanges occur too fast to be studied by presently available experimental techniques [3,14]. Femtosecond laser pulse spectroscopy has been applied to investigate the mean lifetime of bonds and coordination in pure water, yielding a value of 2.0 ps [15], but the application of this technique to solute–solvent interactions still faces unsolved technical problems. Computer simulations [4,18,19], on the other hand, are capable of reproducing the time evolution of chemical systems on a very small time scale such as the picosecond regime, and, thus, detailed investigations of these ultrafast ligand-exchange dynamics can be performed based on computational methods. Whereas experimental methods study systems on the macroscopic scale and thereby automatically average the measured properties over all species present in solution, theoretical models deal with the problem on the microscopic, i.e., the atomic and molecular scale, respectively. This approach gives the unique opportunity to monitor and analyze the behavior of every single molecule and atom within the system independently. As liquids combine the density of solids with the mobility of a gas, an accurate description of all interactions at this level is the key challenge determining the accuracy of simulations.

METHODOLOGIES FOR SIMULATING LIQUID SYSTEMS

It is known from statistical thermodynamics [5,6] that a single structure with a distinct distribution of atoms is an insufficient representation of chemical systems at any temperature above 0 K. As many different arrangements of the molecules and atoms will correspond to the same energy, a collection of representative configurations—an ensemble—is required in order to derive a reliable average description of the system, thus also accounting for the influence of entropy.

The very frequently used method of the QM "geometry optimization" is an inadequate tool for the investigation of liquid-state chemistry, as a single minimum structure does not, in general, correspond to any of the many representative configurations. The application of a polarizable continuum model (PCM) [20] in the minimization procedure in order to model the potential of the surrounding solvent [21] has no influence on this methodical shortcoming. Moreover, PCMs represent the surrounding solvent by a constant continuum and thus affect the calculation by a homogeneous potential. At close distances to the solute, the distribution of the surrounding molecules can by no means be assumed homogeneous, however. Hence, conclusions of theoretical investigations based on geometry optimizations even in combination with PCMs have to be critically assessed.

Methods suitable for collecting multiple configurations of an ensemble are known as "statistical simulation methods" [4,18]. Two different approaches exist, the Monte Carlo (MC) and the molecular dynamics (MD) framework. Both methodologies utilize a periodic simulation box (various shapes such as cubes or truncated octahedrons can be employed) to ensure that the simulation corresponds to the situation within bulk. In MC methods in general only a single molecule is moved per step (typically via rotation and/or translation), and the energy difference between the newly generated and the old configuration is considered according to the Metropolis algorithm [22], determining the new configuration's acceptance. MD methods propagate the entire system based on an integration of the Newtonian equations of motions with typical time steps on the femtosecond scale and below. While MC methods require the knowledge of the total energy of the system, MD simulations are based on the forces acting on all particles of the system (the total energy is only required to monitor the stability of the simulation). As MC simulations modify the system randomly, time-dependent properties cannot be evaluated. Nevertheless, MC methods are versatile tools as a large number of different configurations can be quickly compared, which is advantageous in investigations of large biomolecules and docking studies.

Implementations of the MC and MD frameworks are widespread today. One of the main challenges determining the quality of a simulation is the achievable accuracy of energies and forces. In practice, two main approaches exist—molecular mechanics (MM) and quantum mechanics (QM). MM methods are based on parametrized functions representing the interaction between two species. The Lennard–Jones 6–12 potential plus a Coulombic term is one of the simplest potential functions available. Although the construction of the parameters defining the potentials is a difficult, tedious, and, above all, time-consuming task, the accuracy of these approaches is, in general, limited, especially when metal ions are present in the system. Large effort has been devoted to derive better potential forms and parameters, resulting in an enormous amount of literature providing numerous different MM methodologies.

On the other hand, MM methods are computationally very cheap, which is their main advantage for the treatment of large biomolecules such as proteins, nucleic acids, or membranes, which can only be achieved by MM methods to date. Entire sets of balanced parameters are known as *force fields* [23–25], typically parametrized to describe a certain subset of molecules, such as peptides, glycosides, nucleic acids, and membranes. Owing to the complex properties of metal centers in such systems, their parametrization is very challenging, as many body and polarization effects are in general not covered by MM methods, but of high relevance for the chemistry of such centers.

QM methods can overcome these problems as many body and polarization effects are automatically taken into account. QM methods derive energies and forces based on numerical solutions of Schrödinger's equation [26], which are very universal but extraordinarily time-consuming. A large hierarchy of different QM methods exists today [4,8,10] in which accuracy is modestly improving, while the computational demand increases exponentially. A lot of research is devoted to further improvements of the accuracy of QM methods while keeping the associated computational demand within practical limits. Some promising approaches have been formulated which could prove very helpful in the near future [27–29].

Although commercial QM software packages enable a parallel execution of QM calculations utilizing high-performance computing (HPC) clusters, only a small number of particles can be treated, typically up to 100, depending on the accuracy of the QM treatment.

Therefore, compromises between accuracy and computational effort have to be sought. Car–Parrinello (CP) simulations [30] achieve this compromise by employing very simple and time-saving QM methods (namely, density functional theory, or DFT, on the generalized-gradient approximation level such as PBE [31,32] or BLYP [33]) and by a reduction of the number of particles and the simulation time to a (sometimes critical) minimum.

In different studies [34,35], CP simulations have proven to yield data in strong contrast to experimental as well as other theoretical investigations utilizing a more advanced and, therefore, more demanding methodology. In many cases, the shortcomings can be explained by the severe inherent methodical errors of common DFT methods, which have been outlined in detail in a recent report [36].

The reduction of the number of particles sometimes leads to simulation systems which are incapable of even forming a complete second solvation shell and much less, providing a sufficient number of bulk molecules representing the surrounding solvent [37].

A lot of confusion exists with respect to a consistent nomenclature of DFT methods. Although many scientists utilizing DFT methods insist on the usage of the term "ab initio" or "first principle" in connection with DFT methods, the majority of present implementations of density functional theory rely on a number of empirical calibrations, which is in contrast with the dogma of ab initio methods not to use any experimental or empirical data. This applies to the usage as well as to the formulation of the respective methodology, thus characterizing common DFT approaches rather as *semiempirical* methods [36,38–40]. Alternative approaches to formulate true ab initio DFT methods have been presented, however, aiming at the elimination of the severe methodical shortcomings of present DFT implementations and at the same time trying to avoid any calibrations [36,38,39].

Another frequently used ansatz to find a compromise between computational effort and accuracy are hybrid QM/MM methodologies (see Fig. 1) [41–46]. The chemically most relevant system (e.g., an ion and its hydration shell) is treated by QM, while the remaining part of the system is treated by MM. This idea combines the accuracy of QM, namely, the inclusion of all important many-body and polarization effects near the solute with the affordability of MM. Basically, every affordable QM method fulfilling the accuracy requirements can be utilized to describe energy and forces in the QM region. The evaluation of interactions between the two subregions is a challenge, especially if molecules migrate from one zone to the other or bonds are cut by the QM/MM interface.

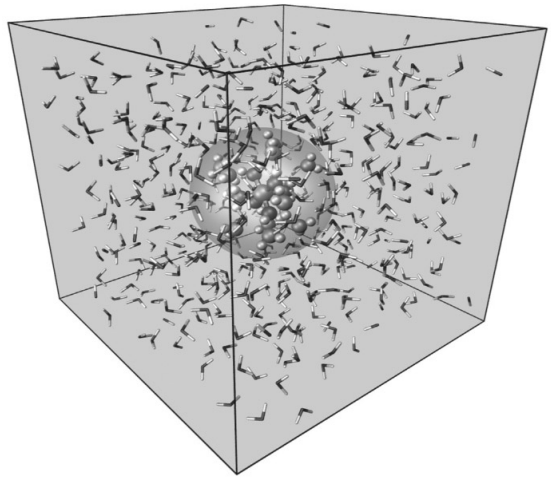

Fig. 1 Scheme of a QM/MM simulation. The chemically most relevant region (indicated by the sphere) is treated at the respective QM level, whereas the interactions in the remaining part of the simulation cube are evaluated by MM.

One critical test scenario to assess the reliability of such methods is the investigation of pure water. The QM/MM MD method was not only able to reliably predict the structural data but also very sensitive dynamical parameters—the MRT, the hydrogen bond lifetime, and the average hydrogen bond number—in excellent agreement with recent experimental studies [47,48]. Investigations of various hydrated ions utilizing the QM/MM ansatz within the MD framework proved to yield reliable data [49,50] if at least double-zeta plus polarization basis sets were utilized in a Hartree–Fock-level treatment. It was also deduced that for some systems the inclusion of the second hydration shell into the QM region is more advantageous than the application of a correlated QM method such as MP/2, which still restricts the manageable size of the QM region to the first hydration shell [47,51]. Apparently, quantum effects

extending beyond the first shell are more important than the small improvements in accuracy achieved by partial inclusion of electron correlation in ion solvates.

Although a large number of simulations have proven the reliability of the QM/MM MD methodology, a more advanced simulation method, the quantum mechanical charge field (QMCF) MD framework [52], was developed to further increase the accuracy, reliability, and applicability of MD simulations. The main increase in accuracy is achieved through an improved coupling of the subregions by inclusion of the point charges of the MM region into the QM treatment. This technique known as *electrostatic embedding* does not significantly extend the computational demand and has been utilized in various investigations [42,53,54], therefore. A further consequence of the improved coupling formulated in the QMCF method is that all interactions between the solute and solvent molecules are taken into account by the QM treatment and the respective CF interaction. Thus, basically any solute can be treated on the basis of this methodology. The number of particles of the solute plus the required number of solvent molecules to hydrate the solute determine the computational effort, which is thus the only limiting factor in the applicability of the QMCF method.

SIMULATION RESULTS

A first example for ligand-exchange reactions is the Cs(I) ion in aqueous solution [55]. Considering the upper limit of the MRT determined by IQENS methods as 200 ps [3], it is evident that this ion is one of the most interesting targets for such studies. Furthermore, the Cs(I) ion is being classified as a "structure breaker" in literature as it is supposed to significantly perturb the water structure instead of forming stable hydrate complexes. Figure 2a depicts the radial distribution functions (RDFs) obtained from

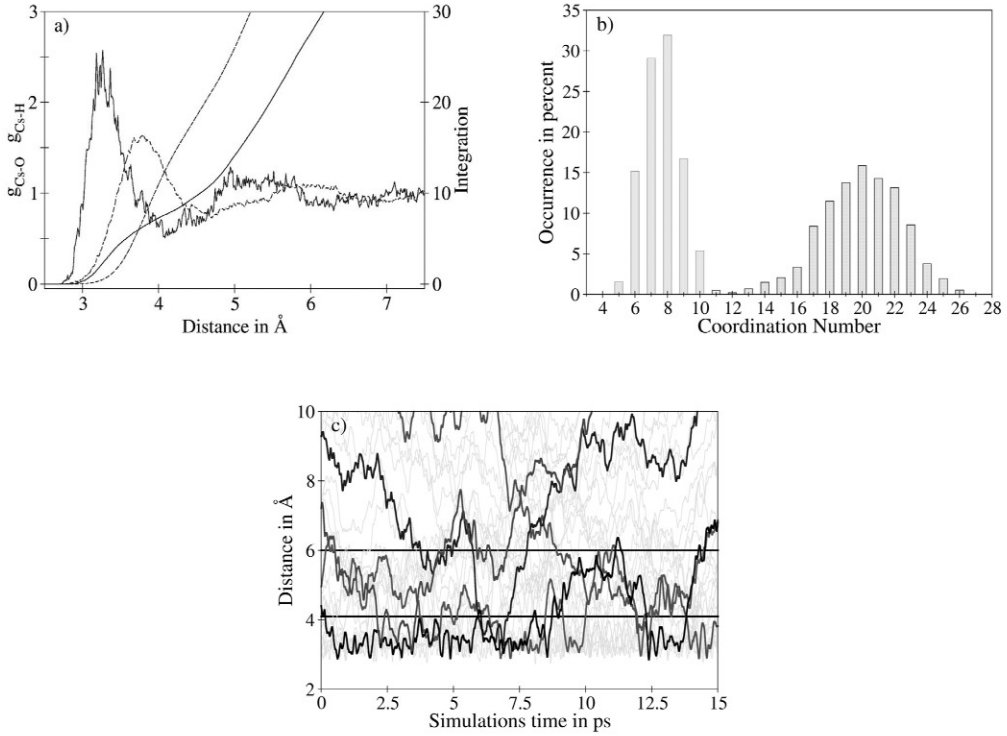

Fig. 2 (a) Cs–O (solid line) and Cs–H (dashed line) RDF, (b) coordination number distribution for the first and second shell, and (c) distance plot for first-shell ligand exchanges obtained from a QM/MM MD simulation of Cs(I) in aqueous solution.

a 15 ps QM/MM MD simulation of Cs(I) in aqueous solution. The bond distance of the first shell of 3.25 Å as well as the first-shell coordination number found as 7.8 are in good agreement with experimental results [56] given as 3.22–3.30 Å for the Cs–O distance and 6–7.9 for the coordination number. However, the considerably high intensity of the minimum between first and second shell indicates that a large number of ligand exchanges took place within the simulation time. The coordination number distributions for the first and second shell given in Fig. 2b reveal a broad distribution of species, and, hence, the value of 7.8 deduced from the RDF has to be considered as an average value. The exchange plot depicted in Fig. 2c demonstrates the ultrafast (i.e., picosecond scale) dynamics of the ligand exchange. During the 15 ps of the simulation, 76 exchange events lasting longer than the critical value of 0.5 ps [57] were registered, resulting in an MRT of 1.5 ps. This value is slightly smaller than the MRT of pure water obtained as 1.7 ps from analogous QM/MM MD simulations [47]. Thus, it can be concluded that the ion accelerates the water molecules' movements in its vicinity rather than forming a stable complex, which appears to be the reason for the "structure-breaking" ability of this particular ion. The MRT value of the second shell was found to be even shorter, namely, 1.3 ps, demonstrating that the structure-breaking effect extends to a larger region.

These findings have some implications for experimental investigations. First, the MRT value deduced from the simulation is significantly smaller than the upper limit deduced from IQENS studies, and hence the exchange rate range for hydrated ions has to be extended from 20 orders of magnitude to 22. Secondly, experimental measurements scanning a sample for a considerably longer time period than the MRT (i.e., hundreds of picoseconds to nanoseconds) will automatically result in an averaged species distribution summarizing a number of different hydrates with varying coordination numbers and associated structures. Even if the experimental technique enables the measurement of dynamics on the subpicosecond scale, the large number of solutes present in solution (typically in the milli- to nanomolar range) will produce a variety of hydrated species, as the ions in solution will show different hydration structures and will not exchange ligands synchronously.

One particular advantage of simulation methods is the distinct evaluation of every configuration, thus enabling the analysis of the species distribution and their individual structures. The detailed treatment of even a single hydrated ion in an environment corresponding to infinite dilution enables the treatment of the system without the influence of counterions. The challenge of simulation work, especially if QM are applied, is to sample a sufficiently large number of configurations to obtain reliable statistics for all properties of interest.

In general, high ligand-exchange rates are a challenge for experimental studies, whose detection limits are typically in the nanosecond region, whereas they are favorable for simulation techniques, as a sufficient number of exchanges can be monitored within a short simulation time. On the other hand, low exchange rates are difficult to evaluate by means of simulations as very long trajectories are required to monitor exchange events.

Simulations of alkaline and alkaline earth ions in aqueous solution underline these conclusions. Table 1 summarizes the first-shell bond lengths, the distribution of the coordination numbers, and the first-shell MRTs. Except in the case of Mg(II) [58], exchange events occur on the picosecond scale, associated with a multispecies distribution. In the case of Ca(II), only three exchange events were monitored along the simulation [59] and due to the associated uncertainty, the estimated MRT for this particular system has to be considered as lower limit.

It can be seen from Table 1 that the MRT values of the alkaline earth ions Sr(II) [60] and Ba(II) [61] are one order of magnitude larger than those of the alkaline ions. Based on the simulation results, the upper limits of the exchange rates deduced from experiments [3,14] are much too high and do not enable a realistic insight into ligand-exchange processes and the properties of these ions in aqueous solution, therefore.

Table 1 Ion–oxygen distance r_1 in Å, distribution of coordination number CN_1 and MRT τ_1 in ps of the first-shell ligands of hydrated alkaline and alkaline earth ions obtained from QM/MM MD simulations.

Ion	r_1	CN_1	τ_1
Na(I)	2.33	4–7	2.4
K(I)	2.81	6–9	2.1
Rb(I)	2.95	4–10	1.9
Cs(I)	3.25	5–10	1.5
Mg(II)	2.05	6.0	–
Ca(II)	2.46	6–9	>43
Sr(II)	2.69	8–10	45
Ba(II)	2.86	8–11	19

Simulations of various other systems were carried out as well in order to investigate whether first-shell ligand exchanges can be observed by means of MD simulations. In QM/MM MD studies of the monovalent ions Ag(I) [62] and Au(I) [63] and the divalent ions Hg(II) [64] and Sn(II) [65] first-shell exchanges were observed on the picosecond scale, whereas ions such as Zn(II) [66] and Pb(II) [67] were found to form stable hydrate complexes which do not exchange ligands within the picosecond scale.

A unique hydration was observed in the case of hydrated Sn(II) [65]. The Sn–O and Sn–H RDFs (cf. Fig. 3a) point toward a regular hydration structure with an average of eight ligands found at a bond length of 2.53 Å with an MRT of 10.0 ps. A detailed analysis of the ion–oxygen bond lengths of the first-shell ligands (see Fig. 3d) has shown that four molecules are strongly bound and did not exchange along the 30.0 ps trajectory, while the remaining ligands (in average, four) are exchanged rapidly with an average MRT value of 5.0 ps. An analysis of the first-shell peak of the ion–oxygen RDF as well as the first-shell ion–oxygen spectrum showed that it is possible to fit two Gaussian peaks with separate peak maxima. Whereas the results are not as good in the case of the ion–oxygen RDF, the fit of the corresponding vibrational spectrum gives an unambiguous result. It has to be mentioned, though, that the fitting of Gaussian functions is a very crude method, and as the peaks show a significant overlap in both cases the standard deviation of the fitted values has to be considered rather high. This MD investigation favorably supplements the conclusions of Ohtaki and coworkers who have assumed four ligands at shorter bond lengths and two other ligands at larger distance, thus resulting in a total coordination number of six [1]. The difference in the coordination numbers from experimental and theoretical data can be explained by the weak bond strength of the ligands with a high exchange rate, which makes the experimental analysis of these ligands difficult. The weak bonding should also be associated with a significant concentration dependence of species. The diffraction study was carried out with concentrated solutions (molar ratio 16.8 and 12.0), which is strongly different from the conditions of the theoretical approach.

Pb(II) did not show any exchange of first-shell ligands [67] although one could expect a shorter first-shell MRT value than for Sn(II), similar to the corresponding ions of the alkaline and alkaline earth series Cs(I) and Ba(II). The stable first-shell hydrate of Pb(II) consisting of nine ligands is characterized, however, by inter-shell motions of the ligands. Water molecules are moving within the first hydration layer, but are not released to the second shell. It appears that these inter-shell migrations are stabilizing the entire hydrate complex and are responsible for the lower exchange rate.

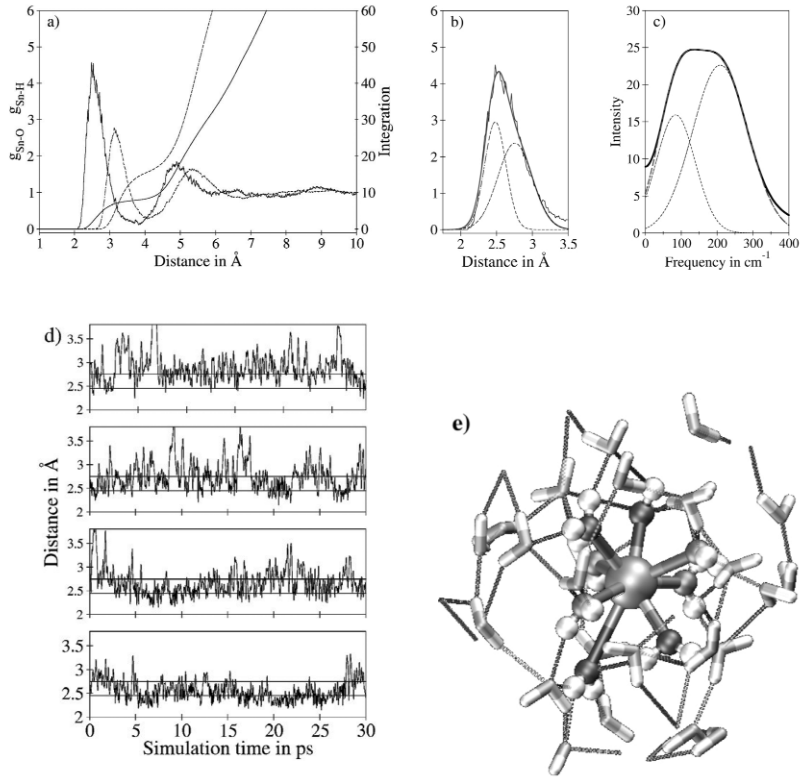

Fig. 3 (a) Sn–O (solid line) and Sn–H (dashed line) RDF of Sn(II) in aqueous solution. Fit of gaussian functions for (b) the Sn–O RDF and (c) the Sn–O vibrational spectrum. (d) Distance plots of the four stable first-shell ligands. (e) Snapshot of the simulation.

A peculiar case is hydrated Cu(II) which shows a distorted first-shell structure resulting from the Jahn–Teller effect [51,68,69]. The ion–water RDF (cf. Fig. 4a) indicates a stable sixfold first-shell hydrate. Ligands in axial positions show an elongated bond, while the remaining four ligands are found at a closer distance. In contrast to Jahn–Teller distorted structures found in crystals, this effect is highly dynamical in solution. Figure 4c shows the O–O distance of opposite ligands within the hydrate complex. The elongation of the bond occurs for all three pairs and is continuously changing from one ligand pair to another.

Due to these rapid variations and the arbitrary definition of the borderline between contracted and elongated positions in some configurations, the number of distant ligands is not exclusively two. As depicted in Fig. 4c, the elongation of the O–O distances of opposite first-shell water molecules are fluctuating on the picosecond scale. It appears that this dynamic Jahn–Teller effect destabilizes the first-shell complex, and thus the exchange rate of the first-shell ligands of Cu(II) is significantly higher than that of other divalent third-row transition-metal ions [3,14]. A similar acceleration of the exchange rate for ligands in elongated axial positions is observed in simulations of Pd(II) and Pt(II), which will be discussed in more detail below.

The bond lengths resulting from the Cu(II) simulations as 1.96/2.3 Å agree well with the experimental values of 2.03/2.3 Å determined by an EXAFS (extended X-ray absorption fine structure) and LAXS (large-angle X-ray scattering) study [70]. The differences of the lower bond length corresponding to the contracted positions can be explained by the dynamics observed in solution. The rapid interchanges from elongated to contracted positions and vice versa influence the average value as does

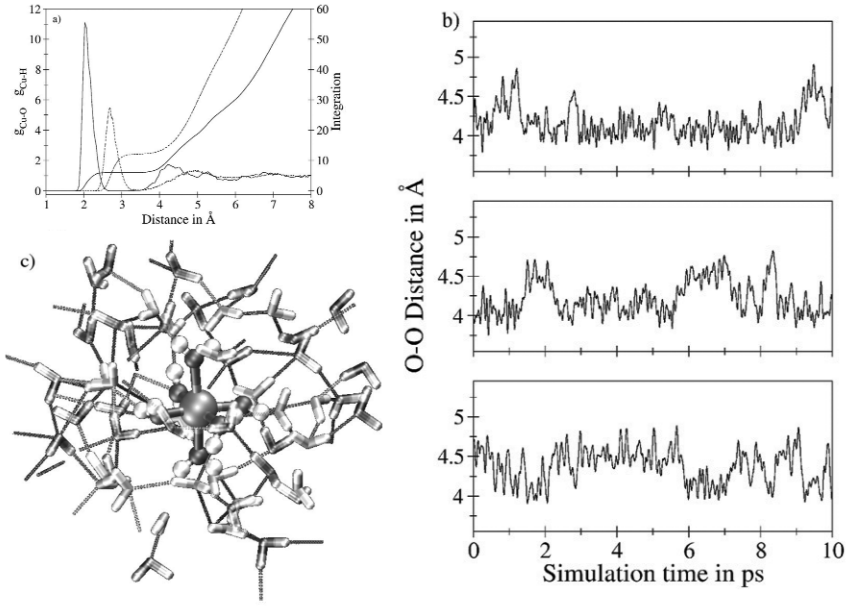

Fig. 4 (a) Cu–O (solid line) and Cu–H (dashed line) RDF of Cu(II) in aqueous solution. (b) Snapshot of the simulaton. (c) Time evolution of the O–O distances of opposing first-shell water molecules.

the definition of the border classifying a ligand as elongated or contracted. The average values of the bond lengths determined from experiment as 2.07 Å and from simulation as 2.11 Å are almost equal. It should be mentioned that only a simulation including the ion and its first plus second hydration shell was able to describe this system accurately [69]. Apparently, quantum effects extending beyond the first shell are essential for the description of this and other Jahn–Teller distorted systems [71].

Another focus of simulation studies was the influence of ammonia ligands on hydration dynamics. Simulations of monoamine, *cis*- and *trans*-diamine complexes of Cu(II) [72] and Zn(II) [73,74] in aqueous solution have been carried out. In the case of the Cu(II)-amine complexes, the sixfold hydration is retained, but the rate constant for water exchanges is increased. The MRT in the case of Cu(II) in aqueous solution was determined as 230 ps by IQENS measurements [75]. The corresponding value in the case of the monoamine complex resulted as 115 ps from a QM/MM simulation study. In the case of the Cu(II)-diamine complexes, the *cis*-compound showed an MRT value of 75 ps, and the *trans*-complex showed the fastest MRT of 35 ps. Hence, the substitution of water ligands by ammonia resulted in a reduction of the water ligand residence time by one order of magnitude. Similar conclusions have been obtained from a QM/MM MD study of Ni(II)-amine complexes in aqueous solution [72].

A different situation was found in the case of Zn(II). Aqueous Zn(II) has a very inert hydration structure [66] with a first-shell exchange rate of 5×10^9 to 10^{10} s^{-1} determined by IQENS studies [76]. Consequently, no first-shell exchange was observed in the QM/MM MD simulation. The replacement of one water by an ammonia ligand did not lead to first-shell exchanges within the simulation time [73]. The substitution of another water by an ammonia molecule led to a decrease of the first-shell coordination number to five [74], i.e., two ammonia and three water ligands formed a stable solvate complexes. In the case of the *cis*-diamine complex, a single exchange of a first-shell ligand was observed. However, after the formation of a four-coordinated transition structure lasting approximately for 4–5 ps, a water molecule entered the first shell, leading to a *trans*-diamine complex. Another simulation starting from the Zn(II)-*trans*-diamine complex showed a very inert first-shell hydration structure which did not show any exchange. Hence, it can be concluded that the Zn(II)-*trans*-diamine complex is the favored and dominant species in aqueous solution.

Investigations of ions in mixed solvents like water/ammonia [77–79] demonstrate another key advantage of simulation methods. Figure 5 displays all RDFs between non-hydrogen atoms observed for Ca(II) in aqueous ammonia [77]. It can be seen that the first-shell RDFs, especially Ca–N, Ca–O, and O–O, strongly overlap. Experimental investigations measure all of these pair distributions simultaneously, and thus the formulation of a suitable solvation model to fit and decompose the measured data is a difficult task. Ligand exchanges leading to a variety of species being simultaneously present in solution further complicate the analysis of experimental spectra. In this and similar cases, simulation methods can provide valuable information for the establishment of suitable models for fitting.

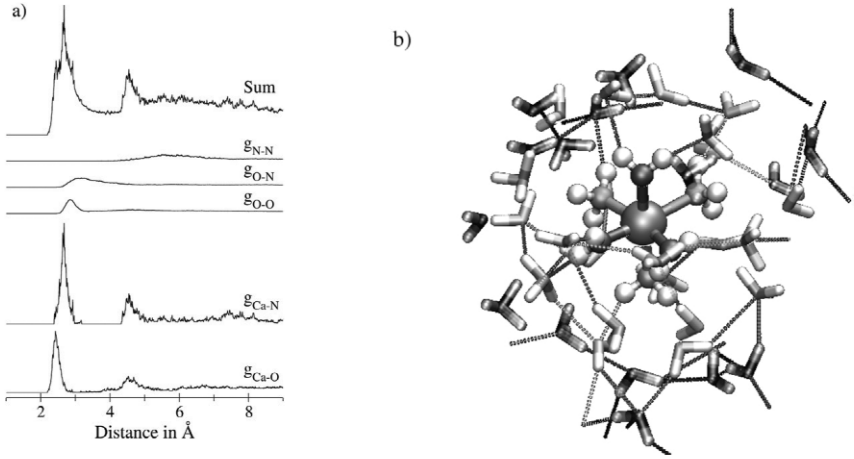

Fig. 5 (a) RDFs of Ca(II) in water/ammonia mixture obtained from a QM/MM MD simulation. (b) Snapshot of the simulation.

The novel QMCF MD methodology [52] has the advantage that no potentials between solvent and solute particles are required, as the associated force contributions are treated by QM and on the basis of partial charges quantum mechanically derived in every simulation step. This opens the possibility to investigate systems whose interactions are difficult to represent by MM potential functions. It should not be concealed that the possibility to renounce solute–solvent potentials is achieved at the price of an extended QM region—typically consisting of the ion and two full layers of hydration—and thus a significant increase of the computational effort.

The first examples demonstrating the capability of the QMCF MD methodology were Pd(II) [80] and Pt(II) in aqueous solution. Until recently, it was believed that the hydrates of these ions are square–planar, similar to their structure in crystals. Recent experimental [81] and theoretical [82] investigations have pointed out that in addition one or two ligands are present in axial positions, i.e., perpendicular to the square–planar arrangement of four water molecules. QMCF MD simulations carried out for both ions have confirmed these conclusions.

Figure 6a depicts the RDFs of Pd(II) and Pt(II) in aqueous solution. After the first-shell peak located at 2.0 and 2.1 Å, a smaller peak is visible at extended bond lengths of 2.70 and 2.75 Å, respectively, corresponding to the ligands in axial positions. This bipyramidal structure is separated from the second hydration shell via a distinct minimum, and hence the second peak has to be attributed to the first shell.

The total first-shell coordination numbers found in the case of Pd(II) and Pt(II) are 5.6 and 5.5. Together with the coordination number distribution, these values indicate the occurrence of ligand exchanges along the simulation. The associated exchange plots reveal a number of exchanges, corresponding to MRTs of 2.8 and 3.9 ps for Pd(II) and Pt(II), respectively. These values are not related to the

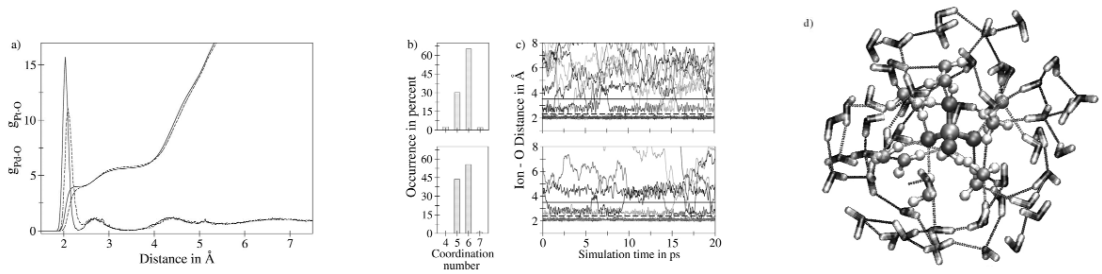

Fig. 6 (a) Pd–O (solid line) and Pt–O (dashed line) RDF, (b) coordination number distribution, and (c) distance plot for first-shell ligand exchanges obtained from QMCF MD simulations of Pd(II) and Pt(II). (d) Snapshot of Pd(II) (aq.).

experimentally determined rate constants being 5.6×10^2 and 3.9×10^{-4} s^{-1} for Pd(II) and Pt(II) [14], respectively, which correspond to the exchange of equatorial ligands. Both the rate constants of the equatorial water molecules and the MRT values of the axial ligands lead to the conclusion that Pt(II) forms a more stable hydrate complex than Pd(II). Recent EXAFS investigations of Pd(II) in aqueous solution have confirmed the predictions obtained from the simulation [80].

The Hg(I) dimer Hg_2^{2+} is another system where the advantages of the QMCF MD methodology can be illustrated. Classical or conventional QM/MM MD frameworks would require solute–solvent interaction potentials, whose construction would be a difficult task in this particular case.

Figure 7a displays the averaged Hg–O and Hg–H RDFs obtained from the QMCF MD simulation. Besides the presence of two well-defined hydration structures, the occurrence of rapid ligand-exchange reactions can be recognized from the non-zero minimum between the first and second shell. The first shell, populated in average by 3.7 water molecules, is located at 2.41 Å in average. The Hg–Hg bond length is 2.60 Å. These values agree with data of a combined EXAFS and LAXS investigation reporting the Hg–Hg and Hg–O distances as 2.52 and 2.24–2.28 Å [83], respectively. The deviation from the latter value can be explained by the occurrence of ligand-exchange reactions shifting the average value to higher distances and partly also by the influence of relativistic effects. Core electrons are most

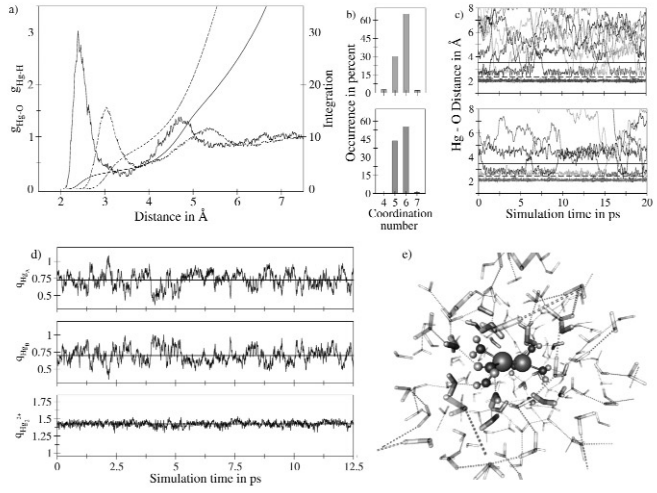

Fig. 7 (a) Averaged Hg–O (solid line) and Hg–H (dashed line) RDF of the Hg(I) dimer in aqueous solution. (b) Coordination number distribution and (c) exchange plots of both Hg atoms, respectively. (d) Partial charges for both Hg atoms as well as the total charge of the Hg_2^{2+} ion. (e) Snapshot of the simulation.

influenced by these effects and, therefore, have been treated via a relativistic effective core potential in the QM formalism. Although the associated contraction of the core electrons is thus included in the QM treatment, the valence electrons are not explicitly treated to include special relativity, which should result in a further contraction of the bond length. However, a full relativistic treatment of this system is unfeasible with the present computational facilities. The different conditions of the experiment and the simulation are also likely to cause deviations. Whereas the simulation corresponds to an infinitely dilute system, a 0.5 M $Hg_2(ClO_4)_2$ solution was employed for the experimental investigations; in order to suppress hydrolysis and disproportionation, 30 % $HClO_4$ had been added to the solution [83]. This amount of acid is likely to influence the hydration as the dielectric constant is strongly influenced by the high concentration of ions, and because the number of water molecules available for hydration is too small to properly form a distinct first and second hydration structure of every ion in the solution. This could also explain the differences in the coordination number, which was given as 3 from the experimental investigations, whereas a value of 3.7 was found from the simulation for dilute condition.

Figure 7b displays the coordination number distributions of both atoms of the Hg(I) dimer. These distributions demonstrate that three-, four-, and fivefold coordination coexist in the simulation, with a slight preference for coordination number 4. The distance plots (Fig. 7c) indicate that the hydration of this ion is highly dynamic, resulting in a average MRT value of 3.0 ps. Besides the evaluation of structural and dynamical data simulations can also yield energetic properties. The average hydration energy of –1137 kJ/mol derived from the simulation is in perfect agreement with the experimental estimation of –1148 kJ/mol based on the TATB (tetraphenylarsoniumtetraphenylborate) assumption [84].

Simulations offer the possibility to monitor data which are not accessible by experiments such as nominal partial charges of the Hg atoms. Figure 7d depicts the partial charges on both Hg atoms as well as the charge of the Hg_2^{2+} ion obtained by Mulliken population analysis [85] during the simulation. All plots have the same scale on the *y*-axes. The charge of the ion displays weak fluctuations around the mean value of 1.43, reflecting the charge transfer from the ion to surrounding solvent molecules. On the other hand, the partial charges of the individual Hg atoms show stronger fluctuations, charge shifts, and spikes. Although the average values are 0.73 and 0.70, respectively, the individual maximum and minimum charges were found to be 1.05 and 0.35. In general, these charge-transfer effects are symmetric—if the charge is rising on one Hg atom it is lowered on the other one and vice versa.

Further test examples for the QMCF MD methodology were composite anions, in particular, phosphate and perchlorate. Potential functions accurately resembling the interaction of these solutes with the solvent are even more complex than for the previous examples. However, since all interactions between phosphate or perchlorate and water are treated by QM, the QMCF MD investigation of these systems is straightforward as well.

Figures 8a and 8b display the RDFs between central atom and water as well as between the anion's oxo-atoms to the O and H atoms of the solvent. All RDFs of the phosphate ion indicate well-defined first- and second-shell structures. In contrast, perchlorate does not form a well-structured first shell, and a second hydration shell can hardly be distinguished from the bulk. The associated MRTs were calculated as 3.9 and 1.5 ps for PO_4^{3-} and ClO_4^-, respectively. Comparison of these data to pure water with its MRT of 1.7 ps [47] allows one to classify perchlorate as "structure breaker", phosphate as "structure former".

Experimental data compare well for both ions. The mean $P–O_{H_2O}$ and $O_{Oxo}–O_{H_2O}$ distances of 3.75 and 1.8 Å coincide with the experimentally determined values [1,86] given as 3.7–3.73 and 1.8 Å and $O_{Oxo}–O_{Oxo}$ Å, respectively. The $P–O_{Oxo}$ distances of 1.57 and 2.57 Å are also predicted in satisfactory agreement with experimental estimations [86] reported as 1.53 and 2.49 Å.

The RDFs in the case of perchlorate pose some difficulties in the evaluation. Even the first-shell peak is not well defined, the respective intensities are only slightly above the value of an ideal gas ($g_{AB} = 1$). It can thus be concluded that the interaction between ClO_4^- and water is very weak, and hence the hydrate is disordered and highly mobile, as already indicated by the MRT. As a consequence, broad plateaus are visible in the RDF rather than distinct peaks. In accordance with this, the experimental

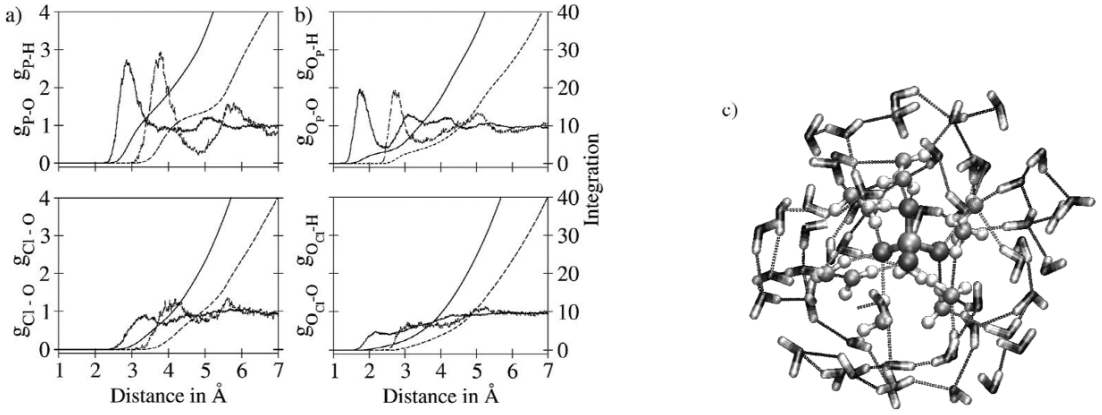

Fig. 8 RDFs of (a) the center atoms and (b) the oxo–atoms to the hydrogen (solid line) and oxygen atoms (dashed line) of water obtained from QMCF MD simulations of PO_4^{3-} and ClO_4^-, respectively. (c) Snapshot of phosphate in aqueous solution.

$Cl–O_{H_2O}$distance, given as 3.6–4.0 Å [1,87,88], has a standard deviation of ~0.3 Å. A distinct maximum is difficult to determine from the RDF of the simulation—only an interval can be given ranging from 3.9 to 4.2 Å. However, the excellent agreement of the $Cl–O_{Oxo}$ distance of 1.45 Å with experimental results reporting 1.43–1.45 Å [87,88] indicates that the simulation reflects the complex situation of this very labile hydrate quite well.

Further analysis of these systems focusing on vibrational as well as energetic properties will give additional data to characterize these complex ionic species. Data obtained from a recent QMCF MD simulation of SO_4^{2-} in aqueous solution are in good agreement with data obtained from LAXS experiments [89]. Further investigations focusing on the hydration energy and vibrational motions of this oxoanion [90] have demonstrated that this novel simulation method allows a thorough study of a variety of properties in a general, accurate, and straightforward way.

CONCLUSION

The QM/MM MD methodology proves to be a versatile technique for the study of solvated species. Especially in cases where high exchange rates and/or a varying preference for ligands result in different simultaneously present solvate species with varying coordination numbers and bond lengths, thus complicating experimental investigations, simulation methods serve as a useful tool to investigate solvation processes. The simulation data support the construction of fitting models and can, therefore, prove essential for an unambiguous evaluation of experimental measurements.

Difficulties in the simulation of systems of low symmetry or of composite compounds have been overcome by the QMCF MD formalism, which is capable of treating all solute–solvent interactions on the basis of quantum mechanics and a fluctuating charge field. The examples presented here make us confident that present ab initio simulation methods exhibit a level of accuracy to reliably predict properties of solvated species. As computational hard- and software resources are constantly improving, the continuous progress in accuracy as well as in applicability of these simulation techniques will be maintained if not accelerated.

ACKNOWLEDGMENTS

Support of this work by the Austrian Science Foundation (FWF) and the Hypo Tirol Bank is gratefully acknowledged.

REFERENCES AND NOTES

1. H. Ohtaki, T. Radnai. *Chem. Rev*. **93**, 1157 (1993).
2. G. W. Neilson, J. E. Enderby. *The Coordination of Metal Aquaions*, Vol. 34, pp. 195–218, Academic Press, Orlando (1989).
3. L. Helm, A. E. Merbach. *Chem. Rev.* **105**, 1923 (2005).
4. M. P. Allen, D. J. Tildesley. *Computer Simulation of Liquids*, Oxford Science Publications, Oxford (1990).
5. McQuarrie. *Statistical Mechanics*, Harper & Row, New York (1976).
6. R. P. H. Gasser, W. G. Richards. *An Introduction to Statistical Thermodynamics*, World Scientific, Singapore (1995).
7. A. J. Stone. *The Theory of Intermolecular Forces*, Oxford University Press, Oxford (1995).
8. A. R. Leach. *Molecular Modelling*, 2nd ed., Prentice-Hall, Essex (2001).
9. F. Jensen. *Introduction to Computational Chemistry*, John Wiley, Chichester (1999).
10. C. J. Cramer. *Essentials of Computational Chemistry*, John Wiley, West Sussex (2002).
11. H. Ohtaki. *Chem. Monthly* **132**, 1237 (2001).
12. G. W. Neilson, A. K. Adya. *Ann. Rep. Chem., Sect. C* **93**, 101 (1996).
13. G. W. Neilson, P. E. Mason, S. Ramos, D. Sullivan. *Philos. Trans. R. Soc. London, Ser. A* **359**, 1575 (2001).
14. L. Helm, A. E. Merbach. *Coord. Chem. Rev*. **187**, 151 (1999).
15. A. J. Lock, S. Woutersen, H. J. Bakker. *Femtochemistry and Femtobiology*, World Scientific, Singapore (2001).
16. P. Wernet, D. Nordlund, U. Bergmann, M. Cavalleri, M. Odelius, H. Ogasawara, L. A. Näslund, T. K. Hirsch, L. Ojamäe, P. Glatzel, L. G. M. Pettersson, A. Nilsson. *Science* **304**, 955 (2004).
17. J. B. R. Bucher, J. Stauber. *Chem. Phys. Lett*. **306**, 57 (1999).
18. D. Frenkel, B. Smit. *Understanding Molecular Simulation*, Academic Press, San Diego (2002).
19. R. J. Sadus. *Molecular Simulation of Fluids*, Elsevier Science, Amsterdam (1999).
20. C. J. Cramer, D. G. Truhlar. *Chem. Rev*. **99**, 2161(1999).
21. F. P. Rotzinger. *Chem. Rev.* **105**, 2003 (2005).
22. N. Metropolis, A. W. Rosenbluth, M. N. Rosenbluth, A. H. Teller, E. Teller. *J. Chem. Phys.* **21**, 1087 (1953).
23. D. A. Pearlman, D. A. Case, J. W. Caldwell, W. Ross, T. Cheatham, S. DeBolt, D. Ferguson, G. Seibel, P. Kollman. *Comp. Phys. Commun*. **91**, 1 (1995).
24. A. D. MacKerell, B. Brooks, C. L. Brooks (III), L. Nilsson, B. Roux, Y. Won, M. Karplus. "CHARMM: The Energy Function and Its Parameterization with an Overview of the Program", in *The Encyclopedia of Computational Chemistry*, John Wiley, Chichester (1998).
25. B. R. Brooks, R. E. Bruccoleri, B. D. Olafson, D. J. States, S. Swaminathan, M. Karplus. *J. Comp. Chem.* **4**, 187 (1983).
26. E. Schrödinger. *Ann. Phys.* **79**, 361 (1926).
27. M. Nooijen. *Phys. Rev. Lett.* **84**, 2108 (2000).
28. H. Nakatsuji. *J. Chem. Phys*. **113**, 2949 (2000).
29. L. Thøgersen, J. Olsen, D. Yeager, P. Jørgensen, P. Salek, T. Helgaker. *J. Chem. Phys.* **121**, 16 (2004).
30. R. Car, M. Parinello. *Phys. Rev. Lett.* **55**, 2471 (1985).
31. J. P. Perdew, K. Burke, M. Ernzerhof. *Phys. Rev. Lett.* **77**, 3865 (1996).
32. J. P. Perdew, K. Burke, M. Ernzerhof. *Phys. Rev. Lett.* **78**, 1396 (1997).
33. A. D. Becke. *Phys. Rev. A* **38**, 3098 (1988).
34. A. Pasquarello, I. Petri, P. S. Salmon, O. Parisel, R. Car, É. Tóth, D. H. Powell, H. E. Fischer, L. Helm, A. Merbach. *Science* **291**, 856 (2001).
35. I. Bakó, J. Hutter, G. Pálinkás. *J. Chem. Phys*. **117**, 9838 (2002).

36. W. Kutzelnigg. *Density Functional Theory (DFT) and ab initio Quantum Chemistry (AIQC): Story of a Difficult Partnership*, G. Maroulis, T. Simos (Eds.), p. 23, International Science Publishers (VSP), Leiden (2006).
37. D. J. Harris, J. P. Brodholt, D. M. Sherman. *J. Phys. Chem. B* **107**, 9056 (2003).
38. R. J. Bartlett, I. V. Schweigert, V. F. Lotrich. *J. Mol. Struct. (Theochem)* **764**, 33 (2006).
39. R. J. Bartlett, V. F. Lotrich, I. V. Schweigert. *J. Chem. Phys.* **123**, 062205 (2005).
40. A. D. Becke. *J. Chem. Phys.* **98**, 5648 (1993).
41. H. M. Senn, W. Thiel. *Curr. Opin. Chem. Biol.* **11**, 182 (2007).
42. H. Lin, D. G. Truhlar. *Theor. Chem. Acc.* **117**, 185 (2007).
43. A. Warshel, M. Levitt. *J. Mol. Biol.* **103**, 227 (1976).
44. M. J. Field, P. A. Bash, M. Karplus. *J. Comput. Chem.* **11**, 700 (1990).
45. J. Gao. *J. Am. Chem. Soc.* **115**, 2930 (1993).
46. D. Bakowies, W. Thiel. *J. Phys. Chem.* **100**, 10580 (1996).
47. D. Xenides, B. R. Randolf, B. M. Rode. *J. Chem. Phys*. **122**, 4506 (2005).
48. D. Xenides, B. R. Randolf, B. M. Rode. *J. Mol. Liq.* **123**, 61 (2006).
49. C. F. Schwenk, A. Tongraar, B. M. Rode. *J. Mol. Liq.* **110**, 105 (2004).
50. B. M. Rode, C. F. Schwenk, T. S. Hofer, B. R. Randolf. *Coord. Chem. Rev.* **249**, 2993 (2005).
51. C. F. Schwenk, B. M. Rode. *J. Am. Chem. Soc.* **126**, 12786 (2004).
52. B. M. Rode, T. S. Hofer, B. R. Randolf, C. F. Schwenk, D. Xenides, V. Vchirawongkwin. *Theor. Chem. Acc.* **115**, 77 (2006).
53. A. Laio, J. VandeVondele, U. Rothlisberger. *J. Chem. Phys.* **116**, 6941 (2002).
54. E. Voloshina, N. Gaston, B. Paulus. *J. Chem. Phys.* **126**, 134115 (2007).
55. C. F. Schwenk, T. S. Hofer, B. M. Rode. *J. Phys. Chem. A* **108**, 1509 (2004).
56. P. R. Smirnov, V. N. Trostin. *Russ. J. Phys. Chem*. **69**, 1097 (1995).
57. T. S. Hofer, H. T. Tran, C. F. Schwenk, B. M. Rode. *J. Comput. Chem*. **25**, 211 (2004).
58. A. Tongraar, B. M. Rode. *Chem. Phys. Lett*. **409**, 304 (2005).
59. C. F. Schwenk, H. H. Loeffler, B. M. Rode. *Chem. Phys. Lett.* **349**, 99 (2001).
60. T. S. Hofer, B. R. Randolf, B. M. Rode. *J. Phys. Chem. B* **110**, 20409 (2006).
61. T. S. Hofer, B. M. Rode, B. R. Randolf. *Chem. Phys*. **312**, 81 (2005).
62. R. Armunanto, C. F. Schwenk, B. M. Rode. *J. Phys. Chem. A* **107**, 3132 (2003).
63. R. Armunanto, C. F. Schwenk, H. T. Tran, B. M. Rode. *J. Am. Chem. Soc.* **126**, 2582 (2004).
64. C. Kritayakornupong, K. Plankensteiner, B. M. Rode. *Chem. Phys. Lett*. **371**, 438 (2003).
65. T. S. Hofer, A. B. Pribil, B. R. Randolf, B. M. Rode. *J. Am. Chem. Soc.* **127**, 14231 (2005).
66. M. Q. Fatmi, T. S. Hofer, B. R. Randolf, B. M. Rode. *J. Chem. Phys.* **123**, 4514 (2005).
67. T. S. Hofer, B. M. Rode. *J. Chem. Phys*. **121**, 6406 (2004).
68. C. F. Schwenk, B. M. Rode. *ChemPhysChem* **4**, 931 (2003).
69. C. F. Schwenk, B. M. Rode. *J. Chem. Phys*. **119**, 9523 (2003).
70. I. Persson, P. Persson, M. Sandström, A.-S. Ullström. *J. Chem. Soc., Dalton Trans.* **7**, 1256 (2002).
71. C. Kritayakornupong, K. Plankensteiner, B. M. Rode. *ChemPhysChem* **5**, 1499 (2004).
72. C. F. Schwenk, T. S. Hofer, B. R. Randolf, B. M. Rode. *Phys. Chem. Chem. Phys*. **7**, 1669 (2005).
73. M. Q. Fatmi, T. S. Hofer, B. R. Randolf, B. M. Rode. *Phys. Chem. Chem. Phys.* **8**, 1675 (2006).
74. M. Q. Fatmi, T. S. Hofer, B. R. Randolf, B. M. Rode. *J. Phys. Chem. B* **111**, 151 (2007).
75. D. H. Powell, L. Helm, A. E. Merbach. *J. Chem. Phys.* **95**, 9258 (1991).
76. P. S. Salmon, M. C. Bellissent-Funel, G. J. Herdman. *J. Phys. Condens. Matter* **2**, 4297 (1990).
77. A. Tongraar, K. Sagarik, B. M. Rode. *Phys. Chem. Chem. Phys*. **4**, 628 (2002).
78. R. Armunanto, C. F. Schwenk, B. R. Randolf, B. M. Rode. *Chem. Phys. Lett.* **388**, 395 (2004).
79. R. Armunanto, C. F. Schwenk, B. M. Rode. *J. Am. Chem. Soc.* **126**, 9934 (2004).
80. T. S. Hofer, B. R. Randolf, S. A. A. Shah, B. M. Rode, I. Persson. *Chem. Phys. Lett.* **445**, 193 (2007).

81. J. Purans, B. Fourest, C. Cannes, V. Sladkov, F. David, L. Venault, M. Lecomte. *J. Phys. Chem. B* **109**, 11074 (2005).
82. J. M. Martinez, F. Torrico, R. R. Pappalardo, E. S. Marcos. *J. Phys. Chem. A* **108**, 15851 (2004).
83. J. Rosdahl, I. Persson, L. Kloo, K. Stahl. *Inorg. Chem. A* **357**, 2624 (2004).
84. M. Yizhak. *Ion Properties*, Marcel Dekker, New York (1997).
85. R. S. Mulliken. *J. Chem. Phys.* **23**, 1833 (1955).
86. P. Mason, J. Cruickshank, G. Neilson, P. Buchanan. *Phys. Chem. Chem. Phys.* **5**, 4690 (2003).
87. G. W. Neilson, D. Schiöoberg, W. Luck. *Chem. Phys. Lett.* **122**, 475 (1985).
88. G. Johansson, H. Wakita. *Inorg. Chem.* **24**, 3047 (1985).
89. V. Vchirawongkwin, I. Persson, B. M. Rode. *J. Phys. Chem. B* **111**, 4150 (2007).
90. V. Vchirawongkwin, B. M. Rode. *J. Phys. Chem.* **10**, 1016 (2007).